Article

Current Biology

Elevated Mitochondrial Bioenergetics and Axonal Arborization Size Are Key Contributors to the Vulnerability of Dopamine Neurons

Highlights

- Vulnerable SNc DA neurons differ in many ways from less vulnerable VTA DA neurons
- SNc DA neurons have a higher basal rate of oxidative phosphorylation (OXPHOS)
- SNc DA neurons have a more complex axon and a higher density of axonal mitochondria
- Reducing axonal arborization size and basal OXPHOS decreases oxidative stress and vulnerability

Authors

Consiglia Pacelli, Nicolas Giguère, Marie-Josée Bourque, Martin Lévesque, Ruth S. Slack, Louis-Éric Trudeau

Correspondence

louis-eric.trudeau@umontreal.ca

In Brief

Pacelli et al. demonstrate that a particularly developed axonal arborization may be at the origin of the vulnerability of substantia nigra dopamine neurons in Parkinson's disease because this morphological characteristic is associated with elevated basal mitochondrial activity and increased oxidative stress.

Pacelli et al., 2015, Current Biology *25*, 2349–2360
September 21, 2015
http://dx.doi.org/10.1016/j.cub.2015.07.050

Current Biology
Article

Elevated Mitochondrial Bioenergetics and Axonal Arborization Size Are Key Contributors to the Vulnerability of Dopamine Neurons

Consiglia Pacelli,[1,4] Nicolas Giguère,[1,4] Marie-Josée Bourque,[1] Martin Lévesque,[2] Ruth S. Slack,[3] and Louis-Éric Trudeau[1,*]

[1]Departments of Pharmacology and Neurosciences, Central Nervous System Research Group (GRSNC), Faculty of Medicine, Université de Montréal, Montréal, QC H4T 1J4, Canada

[2]Department of Psychiatry and Neurosciences, Centre de Recherche de l'Institut Universitaire en Santé Mentale de Québec, Faculté de Médecine, Université Laval, Québec, QC G1J 2G3, Canada

[3]Department of Cellular and Molecular Medicine, Faculty of Medicine, University of Ottawa, Ottawa, ON K1H 8M5, Canada

[4]Co-first author

*Correspondence: louis-eric.trudeau@umontreal.ca

http://dx.doi.org/10.1016/j.cub.2015.07.050

SUMMARY

Although the mechanisms underlying the loss of neurons in Parkinson's disease are not well understood, impaired mitochondrial function and pathological protein aggregation are suspected as playing a major role. Why DA (dopamine) neurons and a select small subset of brain nuclei are particularly vulnerable to such ubiquitous cellular dysfunctions is presently one of the key unanswered questions in Parkinson's disease research. One intriguing hypothesis is that their heightened vulnerability is a consequence of their elevated bioenergetic requirements. Here, we show for the first time that vulnerable nigral DA neurons differ from less vulnerable DA neurons such as those of the VTA (ventral tegmental area) by having a higher basal rate of mitochondrial OXPHOS (oxidative phosphorylation), a smaller reserve capacity, a higher density of axonal mitochondria, an elevated level of basal oxidative stress, and a considerably more complex axonal arborization. Furthermore, we demonstrate that reducing axonal arborization by acting on axon guidance pathways with Semaphorin 7A reduces in parallel the basal rate of mitochondrial OXPHOS and the vulnerability of nigral DA neurons to the neurotoxic agents MPP^+ (1-methyl-4-phenylpyridinium) and rotenone. Blocking L-type calcium channels with isradipine was protective against MPP^+ but not rotenone. Our data provide the most direct demonstration to date in favor of the hypothesis that the heightened vulnerability of nigral DA neurons in Parkinson's disease is directly due to their particular bioenergetic and morphological characteristics.

INTRODUCTION

Parkinson's disease is a chronic progressive neurodegenerative disorder characterized by the selective loss of DA-containing neurons in the SNc (substantia nigra compacta). Although the mechanisms underlying the loss of neurons in idiopathic forms of Parkinson's disease are not well understood, impaired mitochondrial function and pathological protein aggregation are suspected as playing a major role. Why DA neurons and a select small subset of brain nuclei are particularly vulnerable to such ubiquitous cellular dysfunctions is presently one of the key unanswered questions in Parkinson's disease research.

A recent hypothesis proposes that SNc DA neurons are particularly vulnerable because they are autonomous pacemakers dependent on L-type voltage-dependent Ca^{2+} channels of the Cav1.3 type, leading to extensive Ca^{2+} influx and associated ATP-dependent extrusion mechanisms [1–3]. The elevated rate of mitochondrial OXPHOS required to meet the cell's demands in ATP [4] has been hypothesized to lead to oxidative stress and contribute to the heightened vulnerability of these neurons [5].

Another emerging hypothesis proposes that the selectively vulnerability of DA neurons and other cell groups in Parkinson's disease can be explained in large part by the fact that they establish an unusually large axonal arborization and number of axon terminals [6–8]. Such a morphological phenotype can be hypothesized to be associated with particularly high demands in ATP to sustain neurotransmission along profuse axons [9–11].

These two non-mutually excluding hypotheses both imply high energy demands with an expected elevated rate of OXPHOS and associated ROS (reactive oxygen species) production, potentially leading to cellular damage in the context of aging. Crucial key information is presently missing to support this general model of DA neuron vulnerability in Parkinson's disease. So far, no published data have demonstrated that vulnerable DA neurons in the SNc indeed have elevated energetic requirements compared for example to DA neurons of the closely located VTA that are considerably less affected in Parkinson's disease. In addition, no quantitative comparisons have been made comparing the axonal arborization of SNc and VTA DA neurons, and it has never been demonstrated that a large axonal arborization increases basal energetic demands and OXPHOS.

Here, we show that the more vulnerable SNc DA neurons differ from VTA DA neurons in that they show higher basal respiration,

higher axonal mitochondrial density, elevated ROS production, a much more complex axonal arborization, and increased vulnerability to the neurotoxic agents MPP^+ (1-methyl-4-phenylpyridinium), rotenone, and H_2O_2. Furthermore, we provide evidence that manipulating basal energy demands has a predictable effect on neuronal vulnerability. Our data provide strong support in favor of the hypothesis that the particular bioenergetic and morphological characteristics of nigral DA neurons underlie their heightened vulnerability in Parkinson's disease.

RESULTS

SNc DA Neurons Show Elevated Basal Oxidative Phosphorylation and Elevated ROS Production

Experiments were performed using a mouse DA neuron primary culture system in which DA neurons microdissected from the SNc and VTA (Figure S1) were grown on a supporting monolayer of astrocytes. The characteristics of SNc and VTA neurons were also compared to those of olfactory bulb (OB) DA neurons, expected to be quite different because they are local projection neurons and used here as a control, to demonstrate that our model is able to recapitulate some of the known morphological differences between different classes of DA neurons. As a first test of our global hypothesis, we estimated mitochondrial OXPHOS by measuring cellular respiration. We measured both basal and maximal (uncoupled with CCCP) OCR (oxygen consumption rate) in living neurons, examined at 10 days in in vitro (DIV), a time point at which neurons are sufficiently mature and have a large number of functional axon terminals. The OCR measured from purified astrocyte cultures, considerably lower compared to the signal measured from mixed neuron/astrocyte cultures, was subtracted in each experiment to estimate the signal arising from neurons (Figure S2).

An analysis of basal OCR in SNc, VTA, and OB cultures revealed that OCR in SNc neurons was 64.6% higher compared to VTA neurons and more than 4-fold higher (423.2%) compared to OB neurons (Figure 1A). In the presence of the mitochondrial uncoupler CCCP, maximal OCR in SNc and VTA cultures were not statistically different, although they were still elevated compared to OB neurons (Figure 1B). An evaluation of the RCR (respiratory control ratio), calculated as the ratio between basal and maximal OCR, revealed that this ratio was 19.3% lower in SNc compared to VTA neurons, with no statistically significant difference between VTA and OB neurons (Figure 1C). These results suggest that SNc DA neurons are near their maximal capacity at basal state and less capable than other DA neurons of increasing their production of energy when required. Basal glycolysis was not significantly different between SNc and VTA DA cultures (Figure S3A).

Because these primary cultures included other neuron types in addition to DA neurons, we validated our main conclusions using DA neurons purified by fluorescence-activated cell sorting (FACS) from TH-EGFP transgenic mice (Figures 1D–1F). We found that in these cultures, in which all neurons were dopaminergic, the difference in basal OCR between SNc and VTA or OB cultures was even larger than in standard mixed cultures, with SNc DA neurons showing a close to 3-fold increase (274%) relative to VTA or OB (295%) DA neurons (Figure 1D). Importantly, GFP-negative non-DA neurons obtained from the same SNc tissue blocks did not show a similarly elevated basal OCR, thus revealing that the elevated basal OCR in SNc cultures arises specifically from DA neurons (Figure 1D). Additionally, the RCR in purified SNc DA neurons was even smaller than that estimated in mixed cultures, with a value close to 100% (122%), thus further highlighting the fact that SNc DA neurons operate at basal state close to their maximal rate of OXPHOS (Figure 1F). Basal glycolysis was also significantly elevated in purified SNc compared to VTA DA neurons (Figure S3B).

A consequence of OXPHOS is the generation of cellular ROS [12]. Mitochondria are widely recognized as the main source of superoxide in cells [13]. To evaluate whether the elevated OCR in SNc DA neurons resulted in an increased mitochondrial ROS production, we took advantage of the cell-permeant superoxide indicator MitoSOX red, known to selectively target mitochondria where it is rapidly oxidized by superoxide (Figure 1G). Quantification of MitoSOX signal in the axonal domain of SNc and VTA DA neurons revealed highly elevated ROS production in SNc compared to VTA terminals (Figure 1H). Similar results were obtained with the broad-spectrum superoxide sensor DHE (Figure S4).

Elevated OXPHOS and glycolysis in SNc compared to VTA DA neurons could result from activity-dependent mechanisms such as neurotransmitter release [14]. To test this hypothesis, we first examined basal firing rate in these neurons. Patch-clamp recording from GFP-positive DA neurons at 10 DIV (Figure 2A) revealed that the basal firing rate of SNc DA neurons was in fact lower than that of VTA DA neurons (Figure 2B), arguing that an elevated firing rate is not the main explanation for the increased oxidative metabolism in SNc neurons compared to VTA neurons. We next used the sodium channel blocker tetrodotoxin (TTX) (1 μM) to block neuronal firing (complete block after 5 min; n = 10 for SNc and n = 11 for VTA; results not shown). We found that blocking firing caused a significant drop in basal OXPHOS selectively in SNc DA neurons (Figure 2C) without affecting basal ECAR (Figure S3C). In the presence of TTX, basal OCR was not significantly different between SNc and VTA DA neurons (Figure 2D), arguing that a larger proportion of basal OCR in SNc DA neurons derives from activity-dependent cellular processes such as firing and neurotransmitter release.

SNc DA Neurons Display a Larger Axonal Arborization Compared to VTA and OB DA Neurons

Because this parameter is hypothesized to be one of the causes of the elevated metabolic activity of SNc DA neurons, we next compared the size of the axonal arborization of cultured SNc, VTA, and OB DA neurons using semi-automated single neuron tracing (Figure 3A). At 3 and 7 DIV, respectively, the axonal arborization of SNc DA neurons was 113% and 69% larger than that of VTA DA neurons and 545% and 326% larger than that of OB DA neurons (Figures 3B and 3C). Similar differences were observed when comparing the number of axonal processes at 3 and 7 DIV, respectively (Figures 3D and 3E). Confirmatory results were obtained by analyzing axonal complexity using a Sholl analysis (Figure S5). A similar analysis of the dendritic arborization of DA neurons revealed modest differences between SNc and

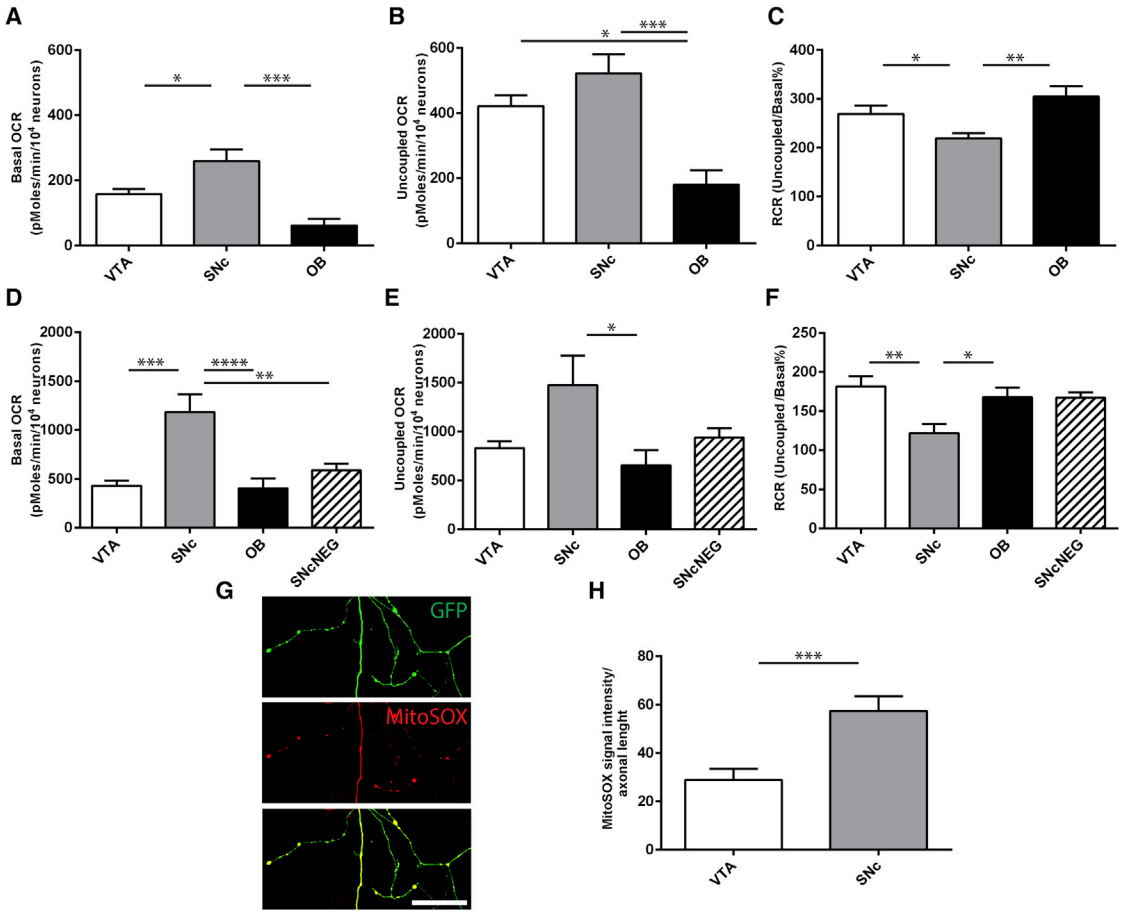

Figure 1. Increased Basal Respiration and ROS Production in SNc Compared to VTA and OB DA Neurons

(A–F) Oxygen consumption rates (OCR) were measured using a XF24 Analyzer from mixed co-cultures (A–C) and FACS-purified DA neurons (D–F) from the VTA, SNc, or OB. Non-DA neurons from the SNc (SNc NEG) were analyzed as a negative control. Basal OCR was measured in mixed co-cultures (A) and FACS-purified DA neurons (D). Maximal or uncoupled OCR was measured in the presence of 0.5 μM CCCP in mixed co-cultures (B) and FACS-purified DA neurons (E). The respiratory control ratio (RCR) was calculated by dividing uncoupled by basal OCR, in mixed co-cultures (C) and FACS-purified DA neurons (F). (The values represent the mean ± SEM, n = 10–30 wells from at least three different cultures. *$p < 0.05$; **$p < 0.01$; ***$p < 0.001$; ****$p < 0.0001$.)

(G and H) Intracellular ROS levels were determined using the superoxide-sensitive fluorescent dye MitoSOX. SNc and VTA DA neurons FACS-purified from TH-GFP mice were incubated with 1 μM MitoSOX for 30 min. (G) Representative confocal images of TH-GFP neurons, axon segments, and MitoSOX fluorescence. Scale bar, 50 μm. (H) Average MitoSOX signal intensity in SNc and VTA DA neurons. Scale bar, 25 μm. The values represent the mean ± SEM, n = 10–15 coverslips from five different cultures *$p < 0.05$; ***$p < 0.001$.

VTA DA neurons at 3 DIV and no significant differences at 7 DIV (Figure S6).

SNc DA Neurons Show an Increased Density of Mitochondria and Elevated ATP Production

An elevated rate of OXPHOS in SNc DA neurons could be due to more active mitochondria, a higher density of mitochondria, or a combination of both. We took advantage of viral-mediated overexpression of DsRed2-mito to visualize the distribution and density of the mitochondrial network in cultured DA neurons (Figure 4A). Mitochondrial density, normalized over process length, was 2-fold higher in the axonal compartment of SNc DA neurons compared to VTA DA neurons (Figure 4B). There was no such difference in the dendritic compartment (Figure 4C) or in the cell body (Figure 4D). This result suggests that the mitochondrial density or content of SNc DA neurons is increased in a spatially restricted manner. Taking into account the previously described increase in SNc axonal arborization size, the difference in total mitochondrial mass is thus expected to be even larger.

As an increase in mitochondrial density and basal rate of OXPHOS is predictive of increased ATP production, we next investigated the relative contribution of mitochondrial OXPHOS to ATP production. We measured intracellular basal ATP content in SNc, VTA, and OB neurons both in the absence and in the presence of oligomycin, a specific inhibitor of the mitochondrial F1F0-ATP-synthase, used here to confirm the involvement of OXPHOS as the source of ATP production. Although it was not possible to distinguish between DA and non-DA neurons, SNc neurons showed a significantly increased oligomycin-sensitive ATP content compared to VTA neurons (Figure 4E), compatible with their elevated basal respiration. Oligomycin induced a decrease of approximately 80% of the levels of cellular ATP

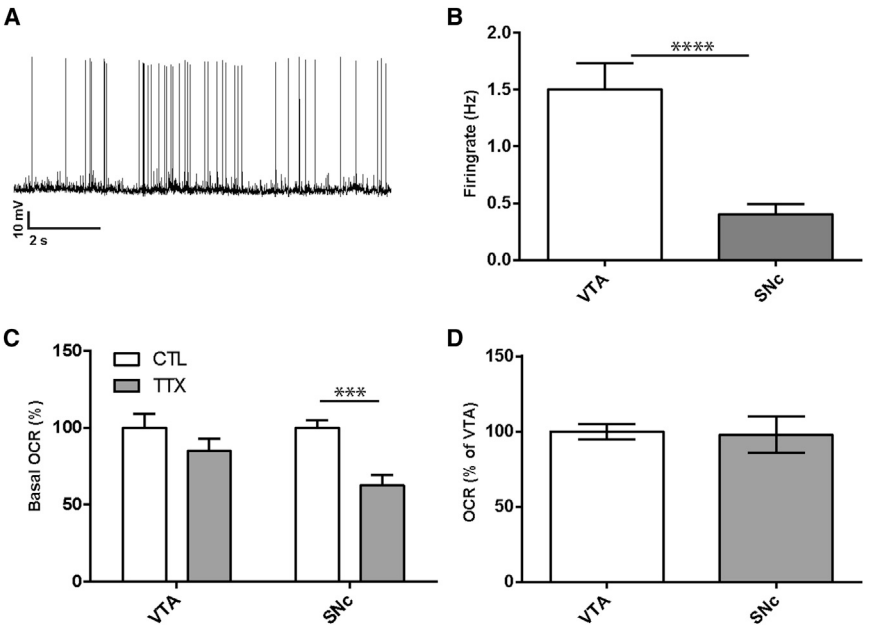

Figure 2. Decreased Basal Firing in SNc Compared to VTA DA Neurons and Effect of TTX on Respiration

(A and B) Firing rates were determined by whole-cell patch-clamping. (A) Representative trace illustrating the basal firing of a cultured DA neuron. (B) Average firing rate of SNc and VTA DA neurons from TH-GFP mice during 10-min recordings. The values represent the mean ± SEM, n = 25 neurons, from at least four different cultures. ****$p < 0.0001$. (C and D) Effect of TTX on basal OCR. After quantifying basal respiration, 1 μM TTX was added to VTA or SNc cultures and the OCR was monitored for 1 hr. The effect of the Na channel blocker on basal respiration was calculated from the ratio of basal OCR to OCR in the presence of TTX. The values represent the mean ± SEM, n = 10–15 wells from four different cultures. ***$p < 0.001$. (D) In the presence of TTX, basal OCR was no longer higher in SNc compared to VTA DA neurons. The values, expressed as percentage of VTA, represent the mean ± SEM (n = 10–15 wells from four different cultures).

(Figure 4F), compatible with a primary role of OXPHOS rather than glycolysis in the production of ATP in our model.

Our observations showing increased mitochondrial density in SNc DA neurons suggest the possibility of an increased rate of mitochondrial biogenesis in these neurons. We used qPCR to examine the level of expression of PGC-1α (peroxisome proliferator-activated receptor γ coactivator), a well-known regulator of mitochondrial function and biogenesis [15]. A significant increase in PGC-1α was detected in SNc DA neurons compared to VTA DA neurons (Figure 4G), compatible with an increased rate of mitochondrial biogenesis in these neurons.

SNc DA Neurons Show Enhanced Vulnerability to Cytotoxic Aggression

SNc DA neurons are well established to be more vulnerable to DA neuron-specific toxins such as 6-OHDA (6-dhydroxydopamine) and MPTP (1-methyl-4-phenyl-1,2,3,6-tetrahydropyridine) or its derivative MPP^+ [16]. However, whether this increased vulnerability is fully cell autonomous and maintained in vitro and whether it is also expressed in response to less selective agents such as mitochondrial toxins is less well established. Following our hypothesis, SNc DA neurons should be more affected by those toxins since they show less respiratory reserve capacity and increased ROS production due to their large bioenergetic requirements. We examined the DA neuron-specific neurotoxin MPP^+, known to be up taken in DA neurons through the DA transporter (DAT) and the membrane-permeable mitochondrial complex-I blocker rotenone. We found that MPP^+ at doses of 5 or 10 μM induced significantly more loss of SNc DA neurons compared to VTA DA neurons (Figure 5A). A similar increased vulnerability was observed for rotenone, tested at 25 and 50 nM, with again the SNc DA neurons being most vulnerable (Figure 5B). Finally, SNc DA neurons were also more vulnerable to direct oxidative stress induced by H_2O_2 (100 μM) (Figure 5C), illustrating that SNc DA neurons show elevated vulnerability to a broad range of cellular stressors, independently of the route of entry or of a direct toxic effect on mitochondria or microtubule function, two cellular targets of MPP^+ and rotenone [17, 18], compatible with their higher basal level of OXPHOS and ROS production.

Implication of L-Type Calcium Channels in Basal Bioenergetics and Vulnerability of SNc but Not VTA Neurons

Following initial experiments evaluating the impact of elevating basal OXPHOS using the AMPK (5′-AMP-activated protein kinase) activator AICAR, which proved unable to reduce vulnerability (Figure S7), we next examined the impact of reducing basal OXPHOS. Elevated intracellular Ca^{2+} resulting from Cav1.3 L-type Ca^{2+}channel activity, a class of channels known to contribute to the pacemaking of SNc DA neurons [3], has been proposed to place a high load on cellular energy stores and contribute to the vulnerability of these neurons [5]. Reducing L-type channel activation is expected to decrease basal OCR in DA neurons, something that has not been previously demonstrated. Reducing activation of L-type Ca^{2+} channels with the negative allosteric regulator isradipine (1 μM) for 1 hr produced a small (22%) but significant reduction in basal OCR in SNc cultures compared to control (Figure 6A). No significant change was detected in VTA neurons. Interestingly, the small reduction in OCR observed in SNc neurons did not abolish the difference in basal OCR between SNc and VTA cultures (Figure 6B), arguing that other factors such as axonal arborization size are important determinants of basal bioenergetic expenditures in SNc DA neurons. As expected from previous studies [19, 20], isradipine had no effect on the average firing rate of SNc or VTA DA neurons (Figure 6C). However, it significantly reduced the vulnerability of SNc DA neurons to MPP^+ (5 μM) (Figure 6D), with 28% more DA neurons surviving in the isradipine-treated group. However, isradipine had

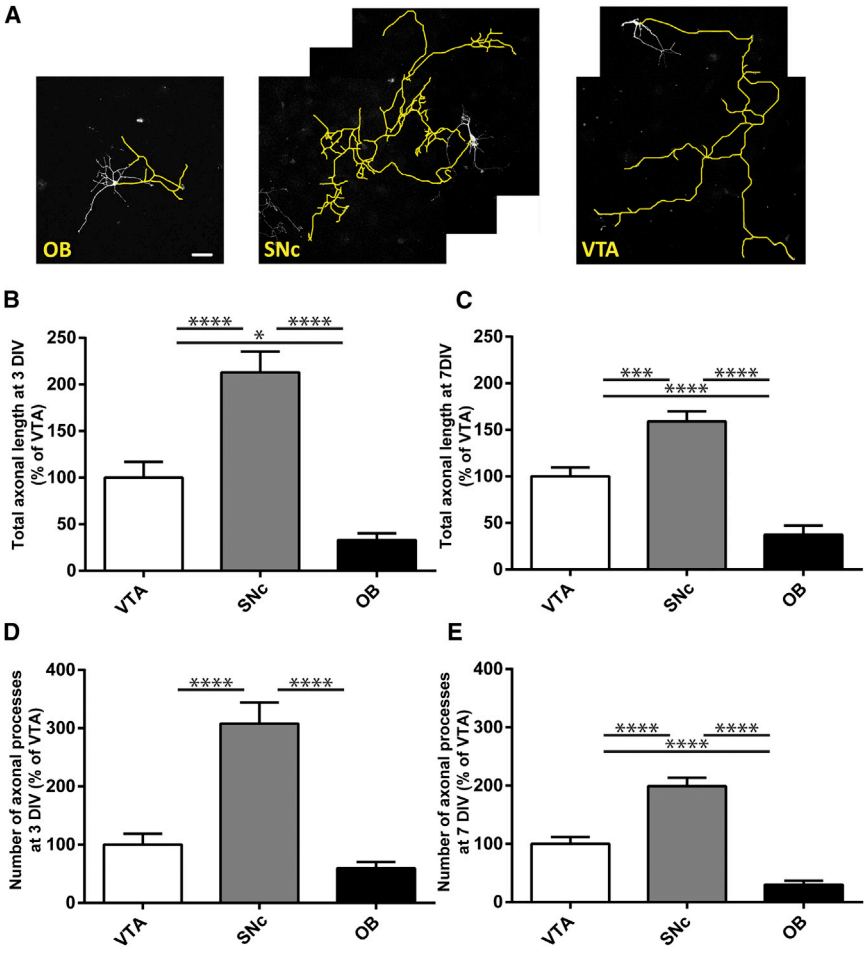

Figure 3. The Axonal Arborization of SNc Neurons Is Larger and More Complex Than That of VTA and OB DA Neurons

The axonal arborization of individual TH-positive DA neurons was measured by semi-automated tracing from confocal image stacks. Isolated DA neurons were randomly selected and imaged by acquiring confocal z stacks at 20×. The longest process, which was three to 20 times longer than the others, was considered as the axon. The axonal arborization of cultured SNc, VTA, and OB DA neurons was measured at 3 DIV and 7 DIV. The images show examples of isolated TH immunopositive neurons from each region (A). Scale bar, 100 μm. The total length (B and C) and number of axonal processes (D and E) were measured at 3 and 7 DIV, respectively. The data represent the mean ± SEM, n = 20–35 neurons from four different cultures. *p < 0.05; **p < 0.01; ***p < 0.001; ****p < 0.0001.

no pro-survival effect against rotenone (50 nM) toxicity (Figure 6E), even if applied chronically (Figure 6F).

Sema7A Reduces Axonal Arborization, Basal OXPHOS, and ROS Production in SNc but Not VTA DA Neurons

Recent work has demonstrated the expression of Sema7A in the ventral midbrain [21–23] and the importance of this guidance factor for the axonal arborization of DA neurons (A. Chabrat et al., 2013, Soc. Neurosci., abstract; A. Chabrat and M.L., unpublished data). Here, we examined the possibility to directly manipulate the axonal arborization of DA neurons to allow a more direct test of the hypothesis that the selectively vulnerability of SNc DA neurons is due in part to their larger axonal arborization and associated lower OCR and oxidative stress. Sema7A (0.5 μg/ml at 0 and 5 DIV) significantly reduced the size of the axonal arborization of SNc DA neurons (46%) but not of VTA DA neurons (Figures 7A and 7B). This was not accompanied by any change in dendritic arborization (Figure 7C) or basal survival (Figure 7D). In close parallel to this decrease in axonal arborization, basal OCR was significantly reduced (39%) in SNc neurons treated with Sema7A compared to control (Figure 7E), bringing basal OCR in SNc neurons to a level similar to that of VTA neurons (Figure 7F). A similar tendency was observed for uncoupled OCR (Figure 7G), although this did not reach statistical significance. A significant increase of 51% in the RCR was selectively detected in SNc DA neurons (Figure 7H). Strikingly, Sema7A treatment was neuroprotective, significantly decreasing the vulnerability of SNc DA neurons to both MPP^+ (Figure 7I) and rotenone (Figure 7J). Neuronal survival was increased by 18% in response to MPP^+ and 27% in response to rotenone in the Sema7A-treated groups. To evaluate whether the effect of Sema7A on basal OXPHOS and axonal arborization decreased ROS production, we measured superoxide levels using MitoSOX red and DHE. Quantification of superoxide production using both of these indicators showed a significant reduction after Sema7A treatment only in SNc DA neurons (Figures 7K and 7L).

DISCUSSION

Although a number of hypotheses have been raised, the particular vulnerability of SNc DA neurons remains unexplained and represents a central unresolved question in Parkinson's disease research. A recently proposed hypothesis suggests that the selective vulnerability of SNc DA neurons in Parkinson's disease can be explained in large part by the fact that these neurons have a particularly large axonal arborization and larger energetic requirements than less vulnerable neurons, leading to an increased rate of basal mitochondrial OXPHOS and associated production of ROS [1, 6, 8, 11]. This hypothesis is not yet supported by direct published evidence.

We have here taken advantage of a novel in vitro system allowing direct comparisons of DA neurons from different brain regions at the morphological and bioenergetic levels. In particular, we provide for the first time a comparison of energetic metabolism in vulnerable SNc DA neurons compared to the closely located and less vulnerable VTA DA neurons. We found that SNc DA neurons have significantly elevated basal and uncoupled mitochondrial respiration compared to VTA and OB DA neurons. Our results also highlight that SNc DA neurons have a smaller

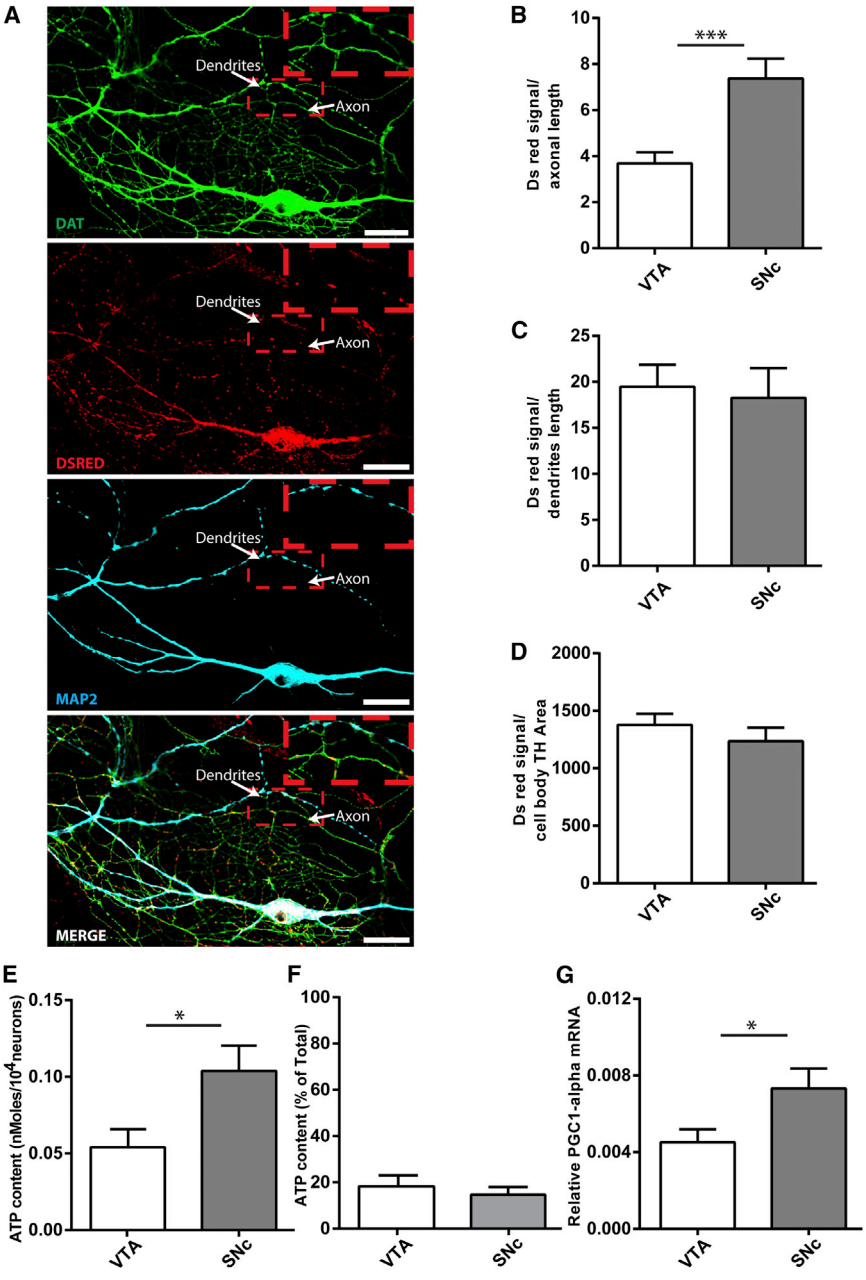

Figure 4. Increased Density of Mitochondria and ATP Content in SNc Compared to VTA DA Neurons

(A–D) Mitochondria were localized in DA neurons after viral infection with mitoDsRed. (A) Representative confocal images from DA neurons immunolabeled with DAT (green), DsRed (red), and MAP-2 (cyan) antibodies. Scale bar, 25 μm, 1.6× zoomed area. The bar graph shows DsRed signal quantified from axons (B), dendrites (C) (normalized on axonal or dendritic length), and the cell body (D) (normalized on TH area). Values represent the mean ± SEM, n = 20–40 neurons from four different cultures. ***p < 0.001.

(E) Oligomycin-sensitive cellular ATP content under basal conditions was quantified in co-cultures prepared from the VTA, SNc, and OB. Values represent the mean ± SEM, n = 6 coverslips from six different cultures. *p < 0.05.

(F) Oligomycin-insensitive cellular ATP content under basal conditions was quantified after incubation with 1 μg/ml oligomycin for 30 min. Values, expressed as percentage of the total ATP content, represent the mean ± SEM, n = 6 coverslips from six different cultures.

(G) PGC-1α mRNA levels were determined by real-time qPCR from total RNA extracted from pools of ten TH-GFP DA neurons. Values were normalized to GAPDH. Values represent the mean ± SEM, n = 15 samples from five different cultures. *p < 0.05.

respiratory control ratio than VTA DA neurons and show an elevated ATP content and basal glycolytic flux (Figure S3). These findings suggest that, at basal state, DA neurons already operate near the maximum of their mitochondrial energy production capacity. This is not the case for glycolysis, which appears to be playing a more modest role in energy production at basal state (but see [14]). The combination of a chronically elevated level of ROS production together with a very small reserve capacity may make it difficult for these neurons to cope with activity-dependent fluctuations in bioenergetic demands as well as with various cellular stresses of genetic or environmental origin or associated with aging. Our second major observation is that SNc DA neurons have a much higher intrinsic capacity for axonal growth than the closely located VTA DA neurons. Together with our results showing that reducing axonal arborization size with Sema7A causes a corresponding decrease in basal OXPHOS and vulnerability, our findings are compatible with the hypothesis that the development of a very large axonal arborization is one of the main reasons underlying the elevated bioenergetic demands of these neurons, thereby placing them at risk for degeneration.

SNc DA neurons are well known in vivo to be more vulnerable than VTA DA neurons to toxins such as 6-OHDA or MPTP [24, 25]. Interestingly, OB DA neurons are also known to be more resistant to such toxins and to be preserved in Parkinson's disease [26, 27]. Although mesencephalic DA neurons in vitro have also been shown to be sensitive to MPP^+ [28, 29], the differential vulnerability of different subtypes of DA neurons in vitro had not been clearly demonstrated. Here, we thus compared for the first time the vulnerability of SNc and VTA DA neurons, showing that, as predicted, SNc DA neurons are more vulnerable to MPP^+. Our finding of a similar increased vulnerability to rotenone, a membrane permeable mitochondrial complex I blocker and H_2O_2, a direct oxidative stressor, further argues that the differential vulnerability of SNc and VTA DA neurons is not simply due to differential expression of DAT, the main port of entry of MPP^+, which is known to be expressed at higher levels in SNc DA neurons relative to the VTA [30].

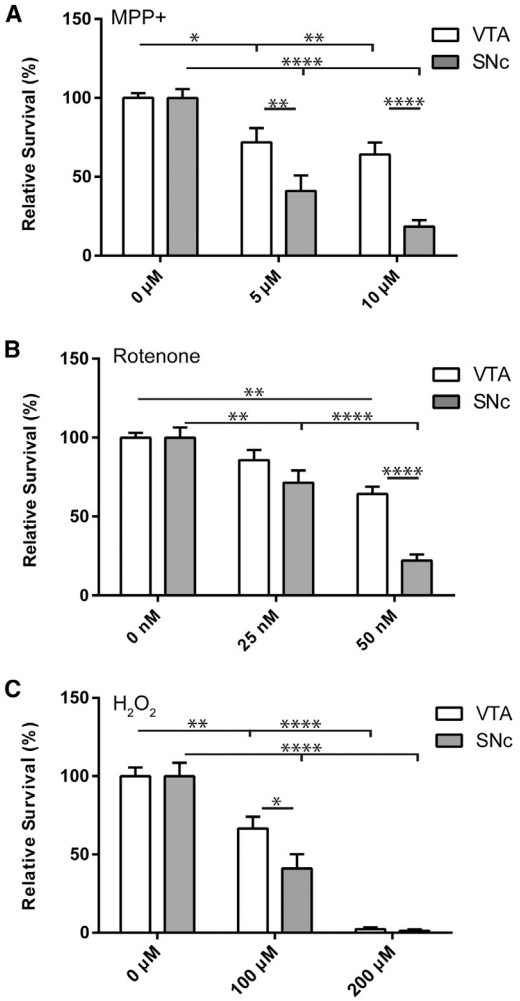

Figure 5. SNc DA Neurons Are More Vulnerable to MPP$^+$, Rotenone, and H_2O_2 Than VTA DA Neurons

(A) SNc and VTA DA neurons were treated with MPP$^+$ (5 and 10 μM, 24 hr), and the proportion of surviving neurons was determined by counting the number of TH-positive neurons with clear round nuclei.

(B) SNc and VTA DA neurons were treated with rotenone (25 and 50 nM, 72 hr) and the proportion of surviving neurons was determined.

(C) SNc and VTA DA neurons were treated with H_2O_2 (100 and 200 μM, 24 hr) and the proportion of surviving neurons was determined. Values represent the mean ± SEM, n = 10–15 coverslips from at least three different cultures. *p < 0.05; **p < 0.01; ****p < 0.0001.

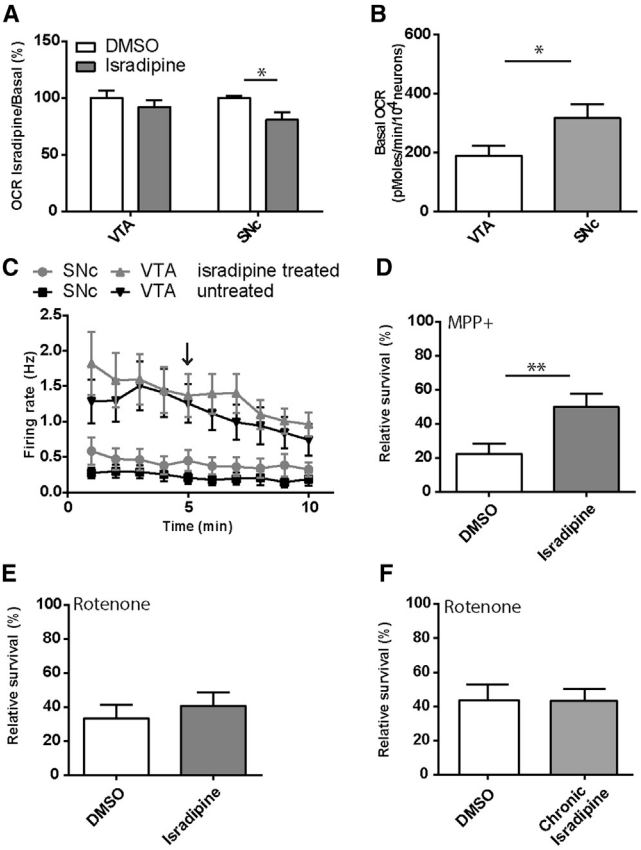

Figure 6. The L-Type Calcium Channel Blocker Isradipine Reduces Basal Respiration and Vulnerability to MPP$^+$

(A) After quantifying basal respiration, 1 μM isradipine was added to VTA or SNc cultures, and the OCR was monitored for 1 hr. The effect of the channel blocker on basal respiration was calculated from the ratio of basal OCR to OCR in the presence of isradipine. The values represent the mean ± SEM, n = 10–15 wells from four different cultures. *p < 0.05.

(B) In the presence of isradipine, basal OCR was still significantly higher in SNc compared to VTA DA neurons. The values represent the mean ± SEM, n = 10–15 wells from four different cultures and statistically analyzed using a t test. *p < 0.05.

(C) The effect of isradipine on firing rate was measured using whole-cell patch-clamp recording from SNc or VTA neurons cultured from TH-GFP mice. After 5 min of baseline recording, isradipine was added for another 5 min (arrow). The values (average firing rate per one min bins) represent the mean ± SEM, n = 15–20 neurons from at least four different cultures.

(D–F) The vulnerability of SNc DA neurons to MPP$^+$ (5 μM, 24 hr) (D) or rotenone (50 nM, 72 hr) (E) was determined after a 3-hr pre-treatment with isradipine (1 μM) or DMSO or (F) in the case of rotenone, after a 3-hr pre-treatment with isradipine (1 μM) or DMSO followed by two additional treatments after 24 and 48 hr. Cells were fixed and TH-positive neurons with clear round nuclei were counted. The values represent the mean ± SEM, n = 15–25 coverslips from three different cultures. **p < 0.01.

Oxidative damage due to mitochondrial dysfunction has been proposed to play an important role in Parkinson's disease pathogenesis [31]. In the present work, we found that ROS content was higher in SNc compared to VTA DA neurons. Using MitoSOX red, we further demonstrate that elevated ROS is likely to be of mitochondrial origin and to occur in axon terminals. Our results are compatible with the hypothesis that increased OXPHOS in SNc DA neurons is the main cause of the elevated ROS levels. Our finding of increased mitochondrial density in these neurons also supports this hypothesis. However, our results do not exclude that, in addition, other sources of ROS such as those arising from the oxidative metabolism of DA itself [32] could also play a role.

A critical question is why DA neurons of the SNc have larger energetic requirements. A recent hypothesis proposes that a common characteristic of vulnerable neurons in Parkinson's disease is that they have a particularly large axonal arborization and a large number of axon terminals [6, 7, 9]. Such a large axonal arborization and number of axon terminals would, in turn, place a large energetic burden on these neurons because of the need

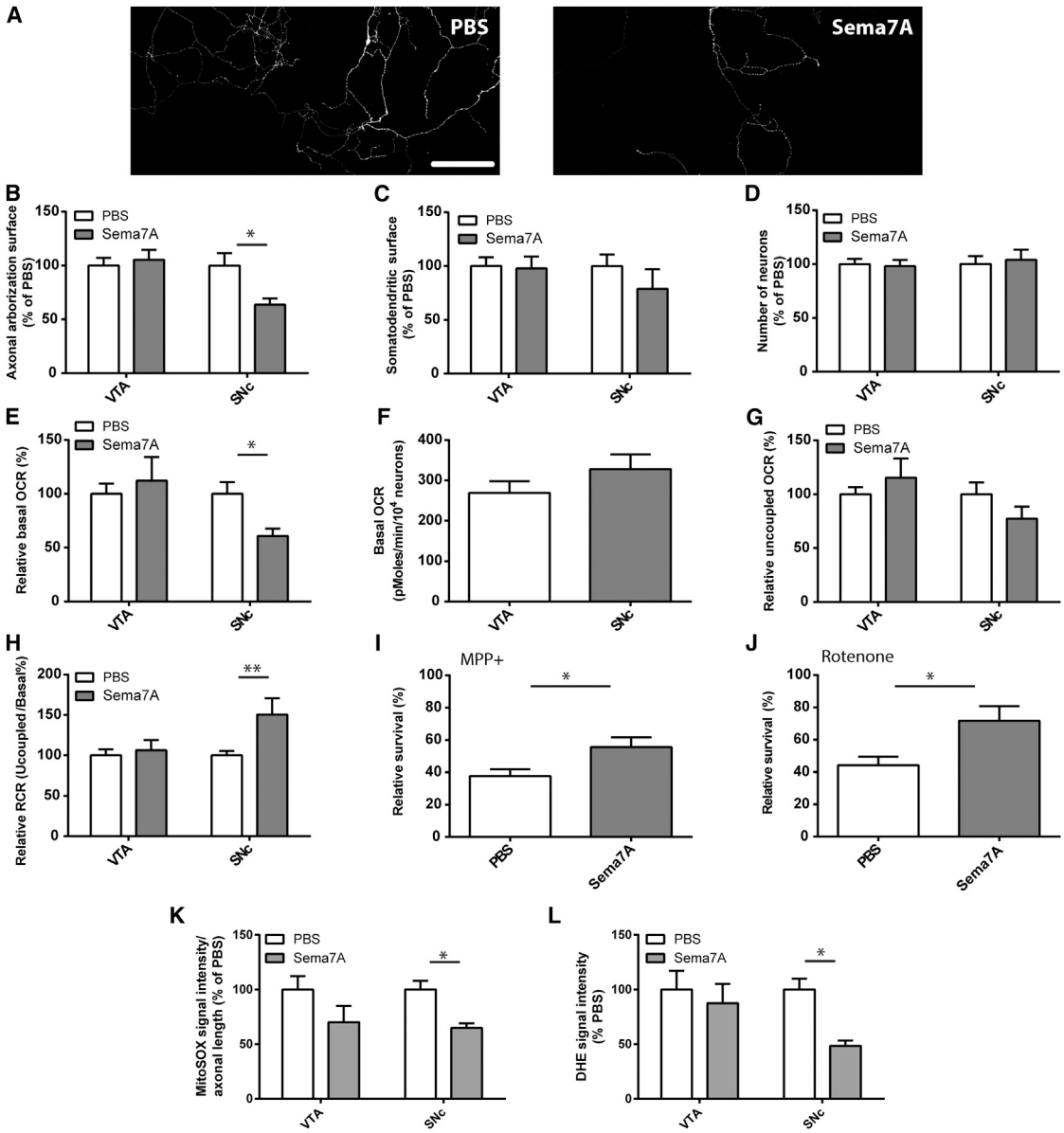

Figure 7. Sema7A Reduces Axonal Arborization Size, Basal OCR, ROS Production, and Vulnerability of SNc DA Neurons

Sema7A (0.5 μg/ml) was added to the cultures at the time of cell plating and at 5 DIV. Neurons were subsequently evaluated at 10 DIV to quantify changes in basal survival and axonal arborization.

(A) Example of axonal TH-immunolabeling of SNc DA neurons after chronic treatment with vehicle (left) or Sema7A (right). Scale bar, 100 μm.

(B) Quantification of axonal arborization surface. The values obtained were normalized to the number of TH-positive neurons.

(C) Quantification of dendritic surface. The values obtained were normalized to the number of TH-positive neurons.

(D) Quantification of the number of TH-positive neurons in VTA and SNc cultures. The values represent the mean ± SEM, n = 15 coverslips from four different cultures. *$p < 0.05$.

(E–H) At 10 DIV, the effect of Sema7A treatment on basal OCR (E and F), uncoupled OCR (G), and RCR (H) was also measured. The values represent the mean ± SEM, n = 15–20 wells from four different cultures. *$p < 0.05$; **$p < 0.01$.

(I and J) The effect of Sema7A pre-treatment on the vulnerability of SNc DA neurons to MPP^+ (5 μM, 24 hr) (I) or rotenone (50 nM, 72 hr) (J) was quantified. The values represent the mean ± SEM, n = 15–25 coverslips. *$p < 0.05$.

(K and L) Intracellular ROS levels were determined using the superoxide-sensitive fluorescent dyes Mitosox and DHE. (K) Average MitoSOX signal intensity in SNc and VTA DA neurons. The values represent the mean ± SEM, n = 8 coverslips from four different cultures. (L) Average DHE signal intensity in SNc and VTA DA neurons. The values represent the mean ± SEM, n = 30 neurons from six different cultures. *$p < 0.05$.

to maintain functional mitochondria and provide energy to all of these structures [8, 11]. Although highly attractive, this hypothesis was not yet supported by any published evidence. In particular, no quantitative comparisons had been made comparing the axonal arborization of SNc DA neurons to that of less vulnerable DA neurons such as those of the VTA or OB. In addition, it

had not been shown that a large axonal arborization indeed increases basal energetic demands, the rate of OXPHOS and the accumulation of ROS. In the present work, we found that the axonal arborization of SNc DA neurons in vitro is approximately 2-fold larger than that of other DA neurons. This observation not only provides support for the cellular energetics/axonal arborization vulnerability hypothesis, but also suggests that having a large axon arborization is an intrinsic property of these neurons that can be maintained in vitro, even in the absence of their normal target neurons. A large axonal arborization and a high number of axon terminals may underlie elevated energetic expenditures related to action potential conduction and activity-dependent axon terminal function. Compatible with this possibility, we found that blocking the firing of SNc DA neurons with TTX reduced OXPHOS to a level comparable to that of VTA neurons.

The higher energetic requirements of SNc DA neurons in relation to their large axonal arborization could in theory be met by a higher efficiency of mitochondrial ATP production and/or higher mitochondrial content. Our experiments revealed a substantially larger density of mitochondria in the axonal domain of SNc DA neurons compared to VTA DA neurons, with no significant change in the dendrites or cell body. This later finding stands in apparent contradiction with a previous brief report showing that in the brain of three Swiss-Webster mice, the fractional area of the cell body of SNc DA neurons occupied by mitochondria was smaller than that of VTA DA neurons [33]. However, it is unclear whether the fractional area is a reliable indicator of the total mitochondrial mass. Our finding of increased expression of PGC-1α, a well-known master regulator of mitochondrial biogenesis, previously demonstrated to regulate mitochondrial density in neurons [34, 35], is also compatible with the hypothesis of increased mitochondrial biogenesis in SNc compared to VTA DA neurons. Much recent work has explored the involvement of PGC-1α in neurodegenerative diseases [36, 37], although the results of experiments evaluating the effects of overexpressing PGC-1α on the vulnerability of mouse DA have been controversial [34, 38–40]. This may result from the difficulty to increase OXPHOS and ATP production without increasing oxidative stress. Compatible with this conclusion, we found that increasing OXPHOS with AICAR, a well-known activator of AMPK [41, 42], failed to decrease the vulnerability of SNc DA neurons (Figure S7). Although we found that AICAR caused a marked increase in OXPHOS that is likely to result from an increase in mitochondrial biogenesis [42], this increased mitochondrial function did not result in reduced vulnerability against MPP^+ or rotenone (Figure S7), arguing that an increase in basal OXPHOS is not an ideal strategy to promote neuroprotection in SNc DA neurons, a conclusion that is compatible with previous results [34, 40].

A second characteristic that has been proposed to lead to increased energy expenditures and vulnerability in SNc DA neurons is autonomous pacemaking [2, 3, 19]. It has been proposed that the pacemaker firing of SNc DA neurons is dependent on L-type voltage-dependent Ca^{2+} channels of the Cav1.3 type, leading to extensive Ca^{2+} influx [3], and that such elevated Ca^{2+} influx is associated with a considerable metabolic cost and oxidative stress [43]. Although quite attractive heuristically and supported by recent work showing that L-type channel blockade can be neuroprotective [44–46], this hypothesis had not yet been supported by data demonstrating that Ca^{2+} influx through L-type channels in SNc DA neurons indeed increases basal energetic expenditures. Our results showing that the L-type Ca^{2+} channel blocker isradipine reduces basal OCR and is protective against MPP^+ fill this gap and provide support for this hypothesis. However, we found no such protective effect of isradipine on toxicity to rotenone, a finding that is at odds with a previous report [47]. Further experiments will be required to test the possibility that this lack of neuroprotection is due to the broader nature of the action of this toxin.

Our observation that SNc and VTA DA neurons still differ in basal OCR in the presence of isradipine suggest that other factors such as the size of the axonal arborization are likely to be additional key players in determining the vulnerability of SNc DA neurons. Supporting this hypothesis, we found that decreasing axonal arborization size in SNc neurons by treating cells with Sema7A (A. Chabrat et al., 2013, Soc. Neurosci., abstract; A. Chabrat and M.L., unpublished data) dramatically decreased basal OCR, which was associated with increased neuronal survival, in essence switching SNc neurons to a VTA-like phenotype. Further experiments will be required to determine whether the neuroprotection induced by Sema7A is fully attributable to its ability to reduce axonal arborization size. It will also be interesting to determine the contribution of beta1-integrin or plexin C1 receptors in the effects of Sema7A, which is otherwise known to have positive effects of axonal growth in other systems [48, 49] (but see [50]). Finally, the developmental time course of the elevated bioenergetics and axonal characteristics of DA neurons would benefit from more detailed evaluation as the present studies were performed with neurons obtained from neonatal animals.

In summary, our work provides the most direct demonstration that the highly elaborate axonal arborization of SNc DA neurons places these neurons at risk in Parkinson's disease because it greatly increases their basal energy demands, leading to chronically elevated oxidative stress and rendering these neurons more vulnerable to perturbations of mitochondrial function, something that can occur in response to multiple factors including gene mutations, exposure to environmental toxicants, and aging.

EXPERIMENTAL PROCEDURES

Primary Neuronal Cultures and Drug Treatments

Cultures were prepared according to a previously described protocol, with minor variations [51]. Neurons from transgenic mice expressing the GFP gene in catecholamine neurons under the control of TH promoter (TH-GFP mice) [52] were also used in electrophysiology experiments and purified by flow cytometry cell sorting for some of the metabolic flux experiments. In some experiments, MPP^+ (Sigma) (5 or 10 μM) or H_2O_2 (Sigma) (100–200 μM) were added at 10 DIV (days in vitro) for 24 hr. In other experiments, the complex I blocker rotenone (Sigma) (25 or 50 nM) was added at 8 DIV for 72 hr. In some experiments, the L-type Ca^{2+} channel blocker isradipine (Tocris) (1 μM) was added 3 hr before MPP^+ or rotenone for acute treatments. For chronic treatment, isradipine was additionally added after 24 and 48 hr in the presence of rotenone. Acute treatments with AICAR (5-aminoimidazole-4-carboxamide-1-β-D-ribofuranoside) (Sigma) (100 μM) were performed at 7 DIV, and chronic treatments with Sema7A (R&D System) (0.5 μg/ml) were performed directly in the culture medium at the time of culture preparation and again at 5 DIV. After 10 DIV, cells were used either for electrophysiology, metabolic flux experiments, or immunocytochemistry. Cells treated with rotenone

or MPP^+ were fixed at 11 DIV, and cells for single neuron morphologic measurements were fixed after 3 or 7 DIV.

Metabolic Flux Experiments

The rate of oxygen consumption deriving from mitochondrial OXPHOS was assessed using an extracellular flux analyzer (Seahorse Biosciences).

Superoxide Level Determination in Live Primary Neurons

To estimate cellular ROS production, superoxide levels were determined using the fluorescent indicators DHE (dihydroethidium) and MitoSOX.

Electrophysiology

Spontaneous firing rate was recorded in a gap-free protocol and the L-type voltage-dependent Ca^{2+} channel blocker isradipine (1 μM) was added after 5 min.

Immunofluorescence

Primary antibodies used were TH-rabbit (Millipore, 1:2,000), DAT-rat (Chemicon, 1:2,000), MAP-2-mouse (Chemicon, 1:1,000), and RFP-rabbit (Rockland, 1:1,000).

Mitochondrial Network Quantification

Mitochondria were labeled by infecting neurons with a lentivirus encoding DsRed2-mito (mitochondrially targeted red fluorescent reporter protein) at 30 MOI at the time of plating and fixed at 10 DIV. Images were obtained by capturing confocal 1-μm z stacks (10–15 images) at 20×.

Single Neuron Morphology, Global Neuronal Morphology, and Survival Assessment

At 3 and 7 DIV, isolated TH-positive DA neurons were randomly selected and imaged by acquiring confocal z stacks at 20× and analyzed using the NeuronJ plugin for ImageJ to reconstruct the axonal and dendritic arbor of each neuron using semi-automated tracing. When single neuron assessment was not necessary, the global size of the neurons' axonal arborization was estimated by capturing random images throughout the coverslip. These values were then normalized to the number of TH neurons with clear round nuclei on the coverslip, estimated by scanning the coverslip vertically and horizontally (cross-counting) at 20×. The same counting method was used for MPP^+ rotenone and H_2O_2 survival experiments.

Real-Time qPCR

Cells were collected as described previously [53]. Real-time qPCR was performed using an Eco Real-Time PCR System (Illumina) in a volume of 15 μl. The reaction mixture included PerfeCTa SYBR Green FastMix (Quanta Biosciences), 5 μl of cDNA, and 0.3 μM of each primer. CT values for gene products were normalized to GAPDH CT values, and comparisons were made between experimental groups, using the DCT method (CT gene of interest minus CT GAPDH) [54].

Measurement of Total Cellular ATP

Cellular ATP content was determined using the PerkinElmer "ATPlite" kit (PerkinElmer) according to the manufacturer's instructions.

Statistics

Parametric statistical tests were used because samples contained data with normal distributions. Data were always obtained from a minimum of three separate sets of experiments and presented as mean ± SEM. The level of statistical significance was established at $p < 0.05$ in one- or two-way ANOVAs and two-tailed t tests performed with the Prism 6 software (GraphPad, $^*p < 0.05$, $^{**}p < 0.01$, $^{***}p < 0.001$, $^{****}p < 0.0001$). The Tukey post hoc test was used when all the means were compared to each other, and the Sidak post hoc test was used when only subsets of means were compared.

SUPPLEMENTAL INFORMATION

Supplemental Information includes Supplemental Experimental Procedures and six figures and can be found with this article online at http://dx.doi.org/10.1016/j.cub.2015.07.050.

AUTHOR CONTRIBUTIONS

C.P. and N.G. are co-first authors. C.P. designed and performed all the experiments related to mitochondria, analyzed data, and contributed to writing the manuscript; N.G. designed and performed all the experiments related to patch-clamp recording, neuronal imaging, and survival, analyzed data, and contributed to writing the manuscript; M.-J.B. prepared all cell cultures; M.L. contributed to the planning of some of the experiments and contributed to revising the manuscript; R.S.S. provided reagents, contributed to the planning of some of the experiments, and contributed to revising the manuscript; L.-E.T. designed, coordinated, and supervised the project and contributed to writing of the manuscript.

ACKNOWLEDGMENTS

The authors wish to thank Dr. Kazuto Kobayashi from Fukushima University, who provided the TH-GFP transgenic mice, and Dr. David Park from the University of Ottawa for his comments and suggestions throughout this project. We also thank Séverine Maire and Caroline Saumure for their participation in some of the experiments. This work was funded by a grant from the Krembil Foundation and the Brain Canada Foundation as well as by a pilot project grant from Parkinson Society Canada. The GRSNC is supported by an infrastructure grant from the Fonds du Québec en Recherche, Santé (FRQS). C.P. and N.G. both received salary support from Parkinson Society Canada. M.L. was supported by a salary award from the FRQS.

Received: February 5, 2015
Revised: June 10, 2015
Accepted: July 20, 2015
Published: August 27, 2015

REFERENCES

1. Chan, C.S., Gertler, T.S., and Surmeier, D.J. (2010). A molecular basis for the increased vulnerability of substantia nigra dopamine neurons in aging and Parkinson's disease. Mov. Disord. *25* (*Suppl 1*), S63–S70.
2. Guzman, J.N., Sánchez-Padilla, J., Chan, C.S., and Surmeier, D.J. (2009). Robust pacemaking in substantia nigra dopaminergic neurons. J. Neurosci. *29*, 11011–11019.
3. Surmeier, D.J., Guzman, J.N., Sanchez-Padilla, J., and Goldberg, J.A. (2011). The origins of oxidant stress in Parkinson's disease and therapeutic strategies. Antioxid. Redox Signal. *14*, 1289–1301.
4. Viola, H.M., and Hool, L.C. (2010). Cross-talk between L-type Ca2+ channels and mitochondria. Clin. Exp. Pharmacol. Physiol. *37*, 229–235.
5. Surmeier, D.J. (2007). Calcium, ageing, and neuronal vulnerability in Parkinson's disease. Lancet Neurol. *6*, 933–938.
6. Parent, M., and Parent, A. (2006). Relationship between axonal collateralization and neuronal degeneration in basal ganglia. J. Neural Transm. Suppl. 85–88.
7. Matsuda, W., Furuta, T., Nakamura, K.C., Hioki, H., Fujiyama, F., Arai, R., and Kaneko, T. (2009). Single nigrostriatal dopaminergic neurons form widely spread and highly dense axonal arborizations in the neostriatum. J. Neurosci. *29*, 444–453.
8. Bolam, J.P., and Pissadaki, E.K. (2012). Living on the edge with too many mouths to feed: why dopamine neurons die. Mov. Disord. *27*, 1478–1483.
9. Gauthier, J., Parent, M., Lévesque, M., and Parent, A. (1999). The axonal arborization of single nigrostriatal neurons in rats. Brain Res. *834*, 228–232.
10. Perier, C., and Vila, M. (2012). Mitochondrial biology and Parkinson's disease. Cold Spring Harb. Perspect. Med. *2*, a009332.
11. Pissadaki, E.K., and Bolam, J.P. (2013). The energy cost of action potential propagation in dopamine neurons: clues to susceptibility in Parkinson's disease. Front. Comput. Neurosci. *7*, 13.
12. Balaban, R.S., Nemoto, S., and Finkel, T. (2005). Mitochondria, oxidants, and aging. Cell *120*, 483–495.

13. Lenaz, G. (2001). The mitochondrial production of reactive oxygen species: mechanisms and implications in human pathology. IUBMB Life *52*, 159–164.
14. Harris, J.J., Jolivet, R., and Attwell, D. (2012). Synaptic energy use and supply. Neuron *75*, 762–777.
15. Lin, J., Handschin, C., and Spiegelman, B.M. (2005). Metabolic control through the PGC-1 family of transcription coactivators. Cell Metab. *1*, 361–370.
16. Bové, J., Prou, D., Perier, C., and Przedborski, S. (2005). Toxin-induced models of Parkinson's disease. NeuroRx *2*, 484–494.
17. Ren, Y., Liu, W., Jiang, H., Jiang, Q., and Feng, J. (2005). Selective vulnerability of dopaminergic neurons to microtubule depolymerization. J. Biol. Chem. *280*, 34105–34112.
18. Choi, W.-S., Kruse, S.E., Palmiter, R.D., and Xia, Z. (2008). Mitochondrial complex I inhibition is not required for dopaminergic neuron death induced by rotenone, MPP+, or paraquat. Proc. Natl. Acad. Sci. USA *105*, 15136–15141.
19. Chan, C.S., Guzman, J.N., Ilijic, E., Mercer, J.N., Rick, C., Tkatch, T., Meredith, G.E., and Surmeier, D.J. (2007). 'Rejuvenation' protects neurons in mouse models of Parkinson's disease. Nature *447*, 1081–1086.
20. Meredith, G.E., Totterdell, S., Potashkin, J.A., and Surmeier, D.J. (2008). Modeling PD pathogenesis in mice: advantages of a chronic MPTP protocol. Parkinsonism Relat. Disord. *14* (*Suppl 2*), S112–S115.
21. Van den Heuvel, D.M.A., and Pasterkamp, R.J. (2008). Getting connected in the dopamine system. Prog. Neurobiol. *85*, 75–93.
22. Hernández-Montiel, H.L., Tamariz, E., Sandoval-Minero, M.T., and Varela-Echavarría, A. (2008). Semaphorins 3A, 3C, and 3F in mesencephalic dopaminergic axon pathfinding. J. Comp. Neurol. *506*, 387–397.
23. Pasterkamp, R.J., Kolk, S.M., Hellemons, A.J., and Kolodkin, A.L. (2007). Expression patterns of semaphorin7A and plexinC1 during rat neural development suggest roles in axon guidance and neuronal migration. BMC Dev. Biol. *7*, 98.
24. Hung, H.C., and Lee, E.H. (1996). The mesolimbic dopaminergic pathway is more resistant than the nigrostriatal dopaminergic pathway to MPTP and MPP+ toxicity: role of BDNF gene expression. Brain Res. Mol. Brain Res. *41*, 14–26.
25. Luk, K.C., Rymar, V.V., van den Munckhof, P., Nicolau, S., Steriade, C., Bifsha, P., Drouin, J., and Sadikot, A.F. (2013). The transcription factor Pitx3 is expressed selectively in midbrain dopaminergic neurons susceptible to neurodegenerative stress. J. Neurochem. *125*, 932–943.
26. Yu, W.H., Matsuoka, Y., Sziráki, I., Hashim, A., Lafrancois, J., Sershen, H., and Duff, K.E. (2008). Increased dopaminergic neuron sensitivity to 1-methyl-4-phenyl-1,2,3,6-tetrahydropyridine (MPTP) in transgenic mice expressing mutant A53T alpha-synuclein. Neurochem. Res. *33*, 902–911.
27. Huisman, E., Uylings, H.B.M., and Hoogland, P.V. (2004). A 100% increase of dopaminergic cells in the olfactory bulb may explain hyposmia in Parkinson's disease. Mov. Disord. *19*, 687–692.
28. Fukuhara, Y., Takeshima, T., Kashiwaya, Y., Shimoda, K., Ishitani, R., and Nakashima, K. (2001). GAPDH knockdown rescues mesencephalic dopaminergic neurons from MPP+ -induced apoptosis. Neuroreport *12*, 2049–2052.
29. Hashimoto, T., Nishi, K., Nagasao, J., Tsuji, S., and Oyanagi, K. (2008). Magnesium exerts both preventive and ameliorating effects in an in vitro rat Parkinson disease model involving 1-methyl-4-phenylpyridinium (MPP+) toxicity in dopaminergic neurons. Brain Res. *1197*, 143–151.
30. Storch, A., Ludolph, A.C., and Schwarz, J. (2004). Dopamine transporter: involvement in selective dopaminergic neurotoxicity and degeneration. J. Neural Transm. *111*, 1267–1286.
31. Chinta, S.J., and Andersen, J.K. (2008). Redox imbalance in Parkinson's disease. Biochim. Biophys. Acta *1780*, 1362–1367.
32. Graham, D.G. (1978). Oxidative pathways for catecholamines in the genesis of neuromelanin and cytotoxic quinones. Mol. Pharmacol. *14*, 633–643.
33. Liang, C.-L., Wang, T.T., Luby-Phelps, K., and German, D.C. (2007). Mitochondria mass is low in mouse substantia nigra dopamine neurons: implications for Parkinson's disease. Exp. Neurol. *203*, 370–380.
34. Clark, J., Silvaggi, J.M., Kiselak, T., Zheng, K., Clore, E.L., Dai, Y., Bass, C.E., and Simon, D.K. (2012). Pgc-1α overexpression downregulates Pitx3 and increases susceptibility to MPTP toxicity associated with decreased Bdnf. PLoS ONE *7*, e48925.
35. Wareski, P., Vaarmann, A., Choubey, V., Safiulina, D., Liiv, J., Kuum, M., and Kaasik, A. (2009). PGC-1alpha and PGC-1beta regulate mitochondrial density in neurons. J. Biol. Chem. *284*, 21379–21385.
36. Zheng, B., Liao, Z., Locascio, J.J., Lesniak, K.A., Roderick, S.S., Watt, M.L., Eklund, A.C., Zhang-James, Y., Kim, P.D., Hauser, M.A., et al.; Global PD Gene Expression (GPEX) Consortium (2010). PGC-1α, a potential therapeutic target for early intervention in Parkinson's disease. Sci. Transl. Med. *2*, 52ra73.
37. Pacelli, C., De Rasmo, D., Signorile, A., Grattagliano, I., di Tullio, G., D'Orazio, A., Nico, B., Comi, G.P., Ronchi, D., Ferranini, E., et al. (2011). Mitochondrial defect and PGC-1α dysfunction in parkin-associated familial Parkinson's disease. Biochim. Biophys. Acta *1812*, 1041–1053.
38. St-Pierre, J., Drori, S., Uldry, M., Silvaggi, J.M., Rhee, J., Jäger, S., Handschin, C., Zheng, K., Lin, J., Yang, W., et al. (2006). Suppression of reactive oxygen species and neurodegeneration by the PGC-1 transcriptional coactivators. Cell *127*, 397–408.
39. Mudò, G., Mäkelä, J., Di Liberto, V., Tselykh, T.V., Olivieri, M., Piepponen, P., Eriksson, O., Mälkiä, A., Bonomo, A., Kairisalo, M., et al. (2012). Transgenic expression and activation of PGC-1α protect dopaminergic neurons in the MPTP mouse model of Parkinson's disease. Cell. Mol. Life Sci. *69*, 1153–1165.
40. Ciron, C., Lengacher, S., Dusonchet, J., Aebischer, P., and Schneider, B.L. (2012). Sustained expression of PGC-1α in the rat nigrostriatal system selectively impairs dopaminergic function. Hum. Mol. Genet. *21*, 1861–1876.
41. Zong, H., Ren, J.M., Young, L.H., Pypaert, M., Mu, J., Birnbaum, M.J., and Shulman, G.I. (2002). AMP kinase is required for mitochondrial biogenesis in skeletal muscle in response to chronic energy deprivation. Proc. Natl. Acad. Sci. USA *99*, 15983–15987.
42. Jäger, S., Handschin, C., St-Pierre, J., and Spiegelman, B.M. (2007). AMP-activated protein kinase (AMPK) action in skeletal muscle via direct phosphorylation of PGC-1alpha. Proc. Natl. Acad. Sci. USA *104*, 12017–12022.
43. Dryanovski, D.I., Guzman, J.N., Xie, Z., Galteri, D.J., Volpicelli-Daley, L.A., Lee, V.M.-Y., Miller, R.J., Schumacker, P.T., and Surmeier, D.J. (2013). Calcium entry and α-synuclein inclusions elevate dendritic mitochondrial oxidant stress in dopaminergic neurons. J. Neurosci. *33*, 10154–10164.
44. Kupsch, A., Sautter, J., Schwarz, J., Riederer, P., Gerlach, M., and Oertel, W.H. (1996). 1-Methyl-4-phenyl-1,2,3,6-tetrahydropyridine-induced neurotoxicity in non-human primates is antagonized by pretreatment with nimodipine at the nigral, but not at the striatal level. Brain Res. *741*, 185–196.
45. Guzman, J.N., Sanchez-Padilla, J., Wokosin, D., Kondapalli, J., Ilijic, E., Schumacker, P.T., and Surmeier, D.J. (2010). Oxidant stress evoked by pacemaking in dopaminergic neurons is attenuated by DJ-1. Nature *468*, 696–700.
46. Ilijic, E., Guzman, J.N., and Surmeier, D.J. (2011). The L-type channel antagonist isradipine is neuroprotective in a mouse model of Parkinson's disease. Neurobiol. Dis. *43*, 364–371.
47. Yu, X., Li, X., Jiang, G., Wang, X., Chang, H.C., Hsu, W.H., and Li, Q. (2013). Isradipine prevents rotenone-induced intracellular calcium rise that accelerates senescence in human neuroblastoma SH-SY5Y cells. Neuroscience *246*, 243–253.
48. Pasterkamp, R.J., Peschon, J.J., Spriggs, M.K., and Kolodkin, A.L. (2003). Semaphorin 7A promotes axon outgrowth through integrins and MAPKs. Nature *424*, 398–405.
49. Jongbloets, B.C., Ramakers, G.M.J., and Pasterkamp, R.J. (2013). Semaphorin7A and its receptors: pleiotropic regulators of immune cell function, bone homeostasis, and neural development. Semin. Cell Dev. Biol. *24*, 129–138.

50. Uesaka, N., Uchigashima, M., Mikuni, T., Nakazawa, T., Nakao, H., Hirai, H., Aiba, A., Watanabe, M., and Kano, M. (2014). Retrograde semaphorin signaling regulates synapse elimination in the developing mouse brain. Science *344*, 1020–1023.

51. Fasano, C., Thibault, D., and Trudeau, L.-E. (2008). Culture of postnatal mesencephalic dopamine neurons on an astrocyte monolayer. Curr. Protoc. Neurosci *Chapter 3*. Unit 3.21.

52. Matsushita, N., Okada, H., Yasoshima, Y., Takahashi, K., Kiuchi, K., and Kobayashi, K. (2002). Dynamics of tyrosine hydroxylase promoter activity during midbrain dopaminergic neuron development. J. Neurochem. *82*, 295–304.

53. Mendez, J.A., Bourque, M.-J., Dal Bo, G., Bourdeau, M.L., Danik, M., Williams, S., Lacaille, J.-C., and Trudeau, L.-E. (2008). Developmental and target-dependent regulation of vesicular glutamate transporter expression by dopamine neurons. J. Neurosci. *28*, 6309–6318.

54. Livak, K.J., and Schmittgen, T.D. (2001). Analysis of relative gene expression data using real-time quantitative PCR and the 2(-Δ Δ C(T)) Method. Methods *25*, 402–408.

